Journal of Translational Medicine

RESEARCH

Open Access

Fecal microbiota transplantation promotes functional recovery in mice with spinal cord injury by modulating the spinal cord microenvironment

Huan Xie[1†], Hui Zhang[2†], Liyi Zhou[2†], Junjie Chen[2], Shun Yao[2], Quanxin He[2], Zhizhong Li[1*] and Zhilai Zhou[2*]

Abstract

Background spinal cord injury (SCI) disrupts the gut microbiota, worsening the injury's impact. Fecal microbiota transplantation (FMT) is increasingly recognized as a promising strategy to improve neural function post-SCI, yet its precise mechanisms are still far from clear. The present study aims to elucidate how FMT influences motor function recovery and its underlying mechanisms utilizing a SCI mouse model.

Methods Mice with SCI received FMT from healthy donors. We used 16 S rRNA amplicon sequencing to analyze the alterations of gut microbes. Pathological alterations in the spinal cord tissue, including neuronal survival, axonal regeneration, cell proliferation, and neuroinflammation, were assessed among experimental groups. Additionally, RNA sequencing (RNA-seq) was used to explore alterations in relevant signaling pathways.

Results Significant shifts in gut microbiota composition following SCI were observed through 16 S rRNA analysis. On day 7 post-SCI, the FMT group exhibited a significantly higher diversity of gut microbiota compared to the ABX group, with the composition in the FMT group more closely resembling that of healthy mice. FMT promoted neuronal survival and axonal regeneration, leading to notable improvements in motor function compared to control mice. Immunofluorescence staining showed increased neuronal survival, alleviated extracellular matrix (ECM) deposition, diminished glial scar formation, and reduced inflammation in FMT-treated mice. RNA-seq analysis indicated that FMT induced transcriptomic changes associated with material metabolism, ECM remodeling, and anti-inflammatory responses.

Conclusions FMT restored gut microbiota balance in SCI mice, mitigated inflammation, and promoted ECM remodeling, establishing an optimal environment for neural recovery. These findings demonstrated that FMT may represent a valuable approach to enhance functional recovery following SCI.

[†]Huan Xie, Hui Zhang and Liyi Zhou contributed equally to this work.

*Correspondence:
Zhizhong Li
tzzli@jnu.edu.cn
Zhilai Zhou
zhouzhilainba@163.com

Full list of author information is available at the end of the article

Keywords Spinal cord injury, Extracellular matrix, 16S rRNA, Fecal microbiota transplantation, RNA sequencing

Introduction

Spinal cord injury results in not only motor and sensory dysfunction but also autonomic nervous system impairment, significantly impacting the quality of life and mental health of patients [1]. The pathophysiology of SCI is intricate, involving initial mechanical damage followed by secondary processes such as inflammation, cell death, oxidative stress, and the development of glial scars. These ongoing processes can hinder and complicate recovery [2]. Recent reports have increasingly highlighted the role of gut microbiota, the community of microorganisms in the digestive tract, in treating neurological diseases through the regulation of immune response [3, 4]. Dysbiosis of gut microbiota were observed following SCI and is believed to exacerbate the injury and hinder recovery [5, 6]. Investigating the role and mechanisms of gut microbiota in SCI presents a compelling research topic and could provide new therapeutic strategies to enhance recovery.

The digestive tract contains billions of microbes, collectively known as the gut microbiota, which play a vital role in metabolic processes, immune function, and energy absorption [7, 8]. A recent study has shown that SCI causes a significant shift in the gut microbiota in fecal samples, including an increased abundance of pro-inflammatory bacteria such as *Staphylococcus*, *Rikenella*, *Bacteroides*, and *Shigella*, and a decreased abundance of certain anti-inflammatory bacteria [9]. Clinical studies have also demonstrated a significant reduction in overall diversity and an altered structural composition in fecal samples of patients following SCI [10, 11], confirming that the gut microbiota undergoes substantial changes.

Given the dramatic changes in the gut microbiota during disease, restoring its balance through fecal microbiota transplantation (FMT) has naturally attracted attention. This strategy has demonstrated beneficial effects in various central nervous system (CNS) conditions, such as Parkinson's disease, stroke, and Alzheimer's disease [12–15]. For instance, FMT treatment has been shown to suppress inflammatory responses by inhibiting the TLR4/NF-κB pathway and improve motor impairment in Parkinson's disease mice [15]. In Alzheimer's disease models, FMT has reversed alterations in gut microbiota and ameliorated deleterious pathological changes. These studies indicate that replenishing the animals' gut with beneficial microbes might alleviate disease-like pathology in various CNS diseases.

In the context of SCI, previous study has shown that FMT treatment can promote intestinal integrity, increase short-chain fatty acids (SCFAs) levels, and improve motor functional deficits [16]. Recent studies have demonstrated that FMT from uninjured donor rats increased the beneficial bacterium *Akkermansia* in SCI rats and improved pathological changes by regulating IL-17 production [17]. These studies demonstrate the potential of FMT in the treatment of SCI by restoring gut microbiota. However, the mechanisms through which FMT exhibits therapeutic effects need further investigation.

In this study, the effects of FMT on motor function recovery and its underlying mechanisms were investigated in a mouse SCI model. We examined neuronal survival, axonal regeneration, cell proliferation, extracellular matrix deposition, and spinal cord inflammation to explore changes in the spinal microenvironment following FMT. Additionally, the composition of the gut microbiome was analyzed using 16 S rRNA gene amplicon sequencing, and RNA sequencing was employed to identify alterations in signaling pathways associated with neuroinflammation and regeneration.

Methods and materials

Animals

Adult female C57BL/6 mice (22 ± 2 g) were obtained from Zhuhai BesTest Bio-Tech Co., Ltd. (License No. SCXK, 2020-0051) in Zhuhai, China. The mice were housed in groups of five under controlled conditions (20℃-25℃, 12-hour light/dark cycle) with ad libitum access to food and water. All experimental procedures were approved by the Ethics Committee of Guangdong Second Provincial General Hospital. (Approval No. 2023-DW-KZ-091-01).

SCI model

A complete crush injury at T9 was induced using modified forceps under anesthesia with 1–3% isoflurane, as previously described [18]. In brief, after separating the paravertebral muscles, the lamina of T8-T10 was removed. The tips of No. 5 Dumont forceps (F. S. T., CA, USA) were inserted on either side of the ventral spinal cord and clamped for 2 s. After confirming compression, the spinal cord was fully clamped with 0.1 mm tip forceps. The muscle and skin were then sutured, and the mice were kept on a warming blanket for recovery. Postoperatively, mice received daily intraperitoneal injections of 0.05 mg/kg buprenorphine dissolved in 1 ml saline for three days. All experiments adhered to international laws and NIH policies.

Experimental design

A total of 152 mice were randomly assigned to four experimental groups as follows:

(i) Sham Group: Mice underwent a laminectomy without SCI. (ii) SCI Group: Mice received SCI and were administered a vehicle solution (100 µl saline) as

a control. (iii) Gut Microbiome-Depleted Group (ABX Group): Mice were treated with an antibiotic cocktail (0.2 g/l ampicillin, 0.2 g/l metronidazole, 0.2 g/l neomycin, and 0.1 g/l vancomycin) daily in their drinking water for three weeks prior to SCI. This treatment continued throughout the duration of the experiment. (iv) FMT Group: Mice received the same antibiotic cocktail as the ABX group to deplete their gut microbiome. Following depletion, fecal microbiota transplantation (FMT) was administered daily via intragastric gavage (100 µl of resuspended fecal material) from the onset of SCI until the time of sacrifice. Sample sizes for each group were determined based on previous studies [19–21]. Detailed numbers and additional experimental parameters are provided in Additional Table 1.

Fecal transplant material preparation

Fecal material was collected from healthy, age-matched female C57BL/6 mice housed under standardized conditions. To reduce potential circadian rhythm effects, fecal samples were obtained in a specific pathogen-free environment between 07:00–11:00 AM or 03:00–05:00 PM. The collected fecal matter was immediately resuspended at a concentration of 10% weight/volume (w/v) in sterile saline and mixed vigorously. The suspension was then centrifuged at 800 g for 5 min, and the supernatant was collected and used for fecal microbiota transplantation.

Behavioral testing

Motor function and coordination in mice were assessed using the Basso Mouse Scale (BMS) scoring system, Inclined Plane Test, and Footprint Analysis, to comprehensively evaluate recovery following SCI.

Basso mouse scale (BMS) scoring system

Motor function in mice was evaluated using the Basso Mouse Scale (BMS) scoring system, which ranges from 0 to 9, with higher scores indicating better motor function. Assessments were performed prior to injury, weekly thereafter, and twice during the first week post-SCI. Before assessment, mice were placed in an open, flat area and allowed to acclimate for 5 min. Each mouse underwent a 4-minute evaluation period. Two experimenters positioned themselves opposite each other to facilitate accurate assessment of both hind limbs. The evaluation included criteria such as plantar position, ankle joint movement, body coordination, and the ability of the hind limbs to bear weight.

Inclined plane test

The Inclined Plane Test was conducted at 35 days post-injury to evaluate hind limb muscle strength and motor coordination. Adjustable inclined plates covered with rubber pads were used to increase friction. During testing, each mouse was placed on the upper section of the inclined plate with its head facing the elevated side, ensuring that the body's longitudinal axis was aligned parallel to the incline. The tilt angle started at 0° and was progressively increased in 5° increments. The maximum angle at which a mouse could maintain its position for at least 5 s without slipping was recorded. Each mouse underwent three trials, and the average value was used for analysis to ensure result accuracy.

Footprint analysis

Footprint analysis was performed at 35 days post-injury to assess gait characteristics and movement coordination. A continuous tunnel with enclosed walls was prepared to ensure unidirectional walking. A clean white paper was placed beneath the tunnel, and non-toxic dyes were applied to the mice's limbs: red for the forelimbs and blue for the hind limbs. As the mice walked through the tunnel, their footprints were imprinted on the paper, which was collected for analysis. Clear footprints were selected, and the stride length and stride width of the hind limbs were measured and statistically evaluated.

Nissl staining and luxol fast Blue (LFB)

Nissl staining involved 12 µm spinal cord sections stained with methyl violet, differentiated until the background was clear, dehydrated, cleared with xylene, and sealed. Microscopic observation focused on cell bodies and Nissl bodies, with statistical analysis of Nissl body numbers near the lesion center to reflect relative neuronal survival.

LFB staining immersed sections in preheated LFB solution at 65 °C for 4 h, followed by rinsing, rapid differentiation, dehydration, clearing, and sealing. Observations under the microscope assessed the morphology and pathological changes of the myelin sheath.

16 S rRNA gene sequencing

Fecal samples for 16 S rRNA gene sequencing were collected following the same procedure outlined in the "Fecal transplant material preparation" section. Mouse feces were gathered and frozen in liquid nitrogen for analysis by BGI Genomics (Shenzhen, China). DNA extraction, library construction, sequencing, and generation of operational taxonomic units (OTUs) were carried out using Usearch. The RDP classifier was used to provide species information for the OTUs. α-Diversity analysis was conducted with Mothur, β-diversity with QIIME, and microbial function prediction with PICRUSt2. Community composition similarities and differences were visualized with heatmaps.

RNA sequencing analysis

Seven days post-operation, 1 cm sections of spinal cord tissue centered on the injury site were harvested. Total RNA was extracted from these samples using a standard RNA extraction protocol. Following extraction, library preparation was carried out according to the manufacturer's instructions. RNA libraries were analyzed using the G400/T7/T10 platform (BGI-Shenzhen, China). Clean data were processed with SOAPnuke, and gene expression levels were quantified using RSEM. Differential expression analysis was performed using DESeq2. Gene Ontology (GO) and Kyoto Encyclopedia of Genes and Genomes (KEGG) pathway analyses were conducted to elucidate phenotypic changes. Significant terms and pathways were adjusted for multiple comparisons using Q values.

Immunofluorescence staining

At various time points, mice were sacrificed, and 1 cm segments of spinal cord, containing the injury center, were isolated through cardiac perfusion using ice-cold saline and 4% paraformaldehyde (PFA). The spinal cord specimens were post-fixed in 4% PFA overnight. Following fixation, the specimens were dehydrated through a gradient of sucrose solutions and subsequently embedded in Optimal Cutting Temperature (OCT) compound. The embedded tissues were sectioned into 12 μm thick slices using a Multicut microtome (Leica Microsystems). For analysis, median sagittal sections were prepared and subjected to staining procedures. After washing with PBS, sections were blocked with 5% donkey serum (Jackson) for one hour. Primary antibodies were then added and incubated overnight at 4 °C. The primary antibodies used, along with their dilutions, were as follows: NF-H (Rabbit, 1:100, Abcam), NeuN (Mouse, 1:400, Merck Millipore), aCaspase-3 (Rabbit, 1:100, Cell Signaling), IBA1 (Rabbit, 1:500, Wako), GFAP (Mouse, 1:1000, EMD Millipore), CD68 (Rat, 1:200, Bio-rad), Fibronectin (Rabbit, 1:400, Jackson), Collagen I (Rabbit, 1:500, Abcam), PECAM-1 (Mouse, 1:300, BD Biosciences), Ki67 (Rabbit, 1:200, Abcam). Secondary antibodies conjugated with AlexaFluor 488 or AlexaFluor 594 (1:300, Jackson) and DAPI (1:1000, Invitrogen) were applied for one hour at ambient temperature. HE staining was performed according to standard procedures.

Image analysis

Fluorescence images were acquired with a Leica STELLARIS 5 microscope (Leica Microsystems). To ensure seamless integration, Photoshop CC was used to combine the images. The images were subjected to thresholding at a constant setting after being converted to 8-bit. Immunofluorescence mean intensity analyses were performed, calculating the mean intensity of NF-H and PECAM-1 after subtracting background signals. Manual counting of Ki67 + cells and NeuN/aCaspase-3 + neurons was done at magnifications of 100× and 200×, respectively. ImageJ software was utilized to measure the gray values of CD68 + cells at various distances to create distribution curves. For a detailed analysis of vascular orientation, three angle ranges (< 25°, 25°~50°, > 50°) were defined, and statistical analysis was carried out using ImageJ software. To quantify neuronal survival, the relative number of Nissl bodies within each square millimeter was determined around the lesion center (upper left, upper right, lower left, and lower right) using ImageJ software. The analysis was performed at a magnification of 400×, and neuronal density was calculated based on the number of Nissl bodies observed in the selected regions.

Statistical analysis

Data were presented as Mean ± Standard Error of the Mean (SEM). Normality was assessed before conducting parametric analyses. Comparisons between two groups were conducted with unpaired t-tests. BMS scores were analyzed using two-way analysis of variance (ANOVA), with post hoc comparisons performed using Tukey's test. One-way ANOVA was conducted for data involving multiple groups, with subsequent post hoc analysis carried out using Tukey's test. A p-value of less than 0.05 was deemed statistically significant.

Results

SCI induced significant changes of gut microbial composition

We performed 16 S rRNA gene amplicon sequencing to examine changes in gut microbiota following SCI. The results revealed a significant decrease in species diversity in the SCI group, as evidenced by the Chao1($P = 0.00389$) and coverage indices ($P = 0.03546$) (Fig. 1A). Although indices like Ace, Simpson, and Shannon did not reach a statistical significance, they also showed a downward trend (data not shown). β-diversity analysis showed clear differences between the SCI and Sham group ($P = 0.00645$) (Fig. 1B). Principal component analysis (PCA) revealed diverse microbial community structures, with PCA1 and PCA2 explaining 52.77% of the variance, highlighting significant functional differences (Fig. 1C). Partial Least Squares Discriminant Analysis (PLS-DA) and non-metric multidimensional scaling (NMDS) further supported the PCA results, demonstrating distinct separation between the groups (Fig. 1D, E). Hierarchical clustering analysis revealed notable changes at the genus level; After SCI, *Muribaculum*, *Roseburia*, *Turicibacter*, *Paramuibaculum*, *Lactobacillus*, and *Kineothrix* significantly decreased in abundance, while *Schaedlerella*, *Saccharibacteria*, *Ligilactobacillus*, *Anaerotignum*, *Bacteroides*, and *Sporofaciens* significantly increased (Fig. 1F).

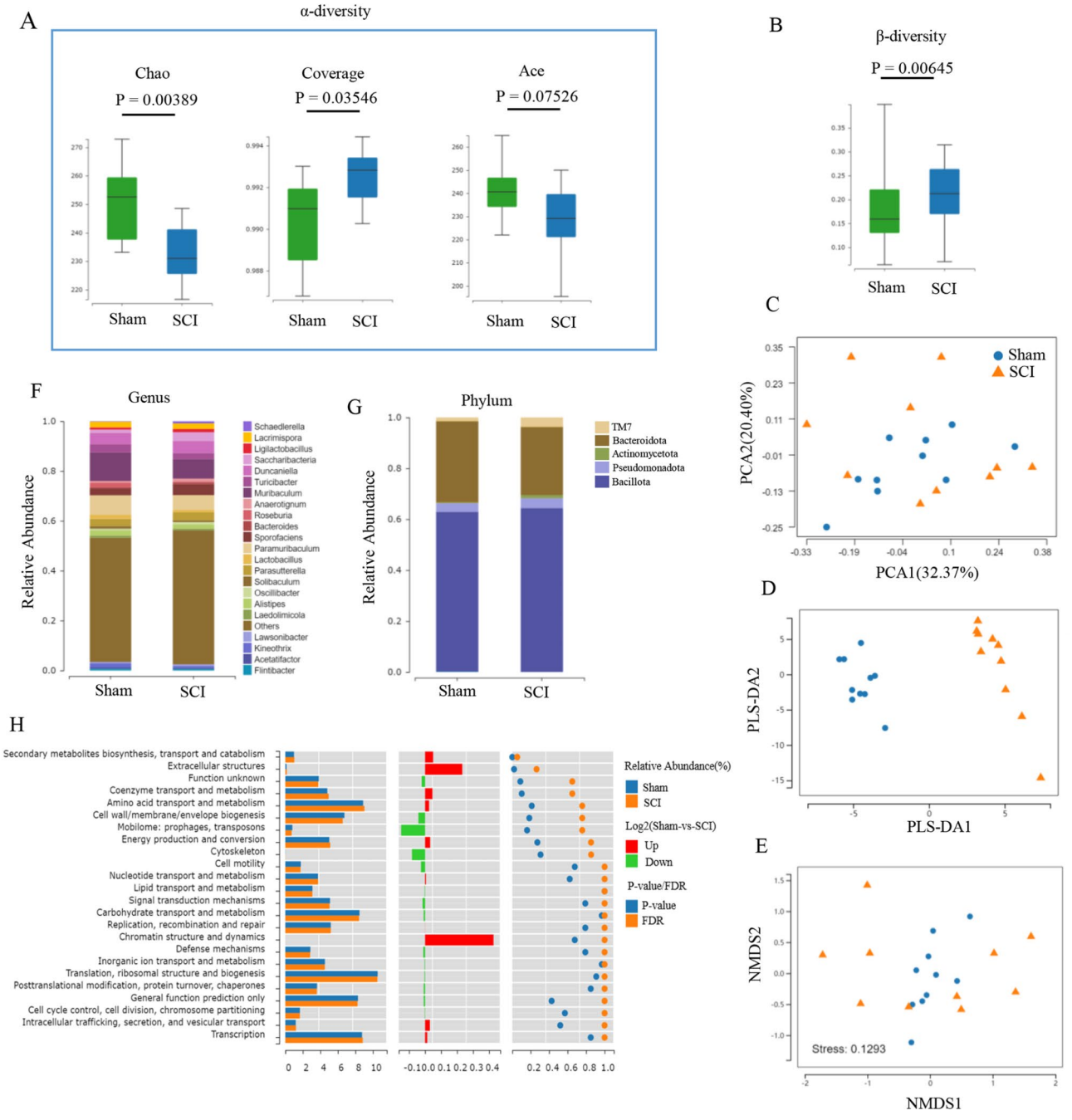

Fig. 1 SCI induced dysbiosis of gut microbiota. **A**. α-diversity indices (Chao, Ace, Coverage) comparing the Sham and injured mice. **B**. β-diversity index showing differences between the SCI and Sham group. **C**. PCA revealed differing microbial community structures between the Sham and SCI groups, with PCA1 and PCA2 explaining 52.77% of the variance. **D**. PLS-DA plot demonstrated a clear distinction between the Sham and SCI mice. **E**. NMDS plot revealed distinct clustering, with Sham and SCI groups occupying distinct regions in the ordination space. Hierarchical clustering analysis of microbial community composition at the genus level (**F**) and the phylum level (**G**) in Sham and SCI groups. **H**. Clusters of Orthologous Groups (COG) function analysis of the Sham and SCI group

At the phylum level, increases in *TM7* (*Saccharibacteria*), *Actinomycetota*, and *Bacillota* following SCI were observed following SCI, while *Bacteroidota* significantly decreased relative to the Sham condition. *Pseudomonadota* abundance showed minimal variation (Fig. 1G). Clusters of Orthologous Groups (COG) analysis indicated that the functional changes due to gut microbiota disturbances were mainly enriched in pathways related to secondary metabolite biosynthesis, transport, and extracellular matrix processes (Fig. 1H). These findings suggest that SCI leads to significant dysbiosis of the intestinal flora in mice.

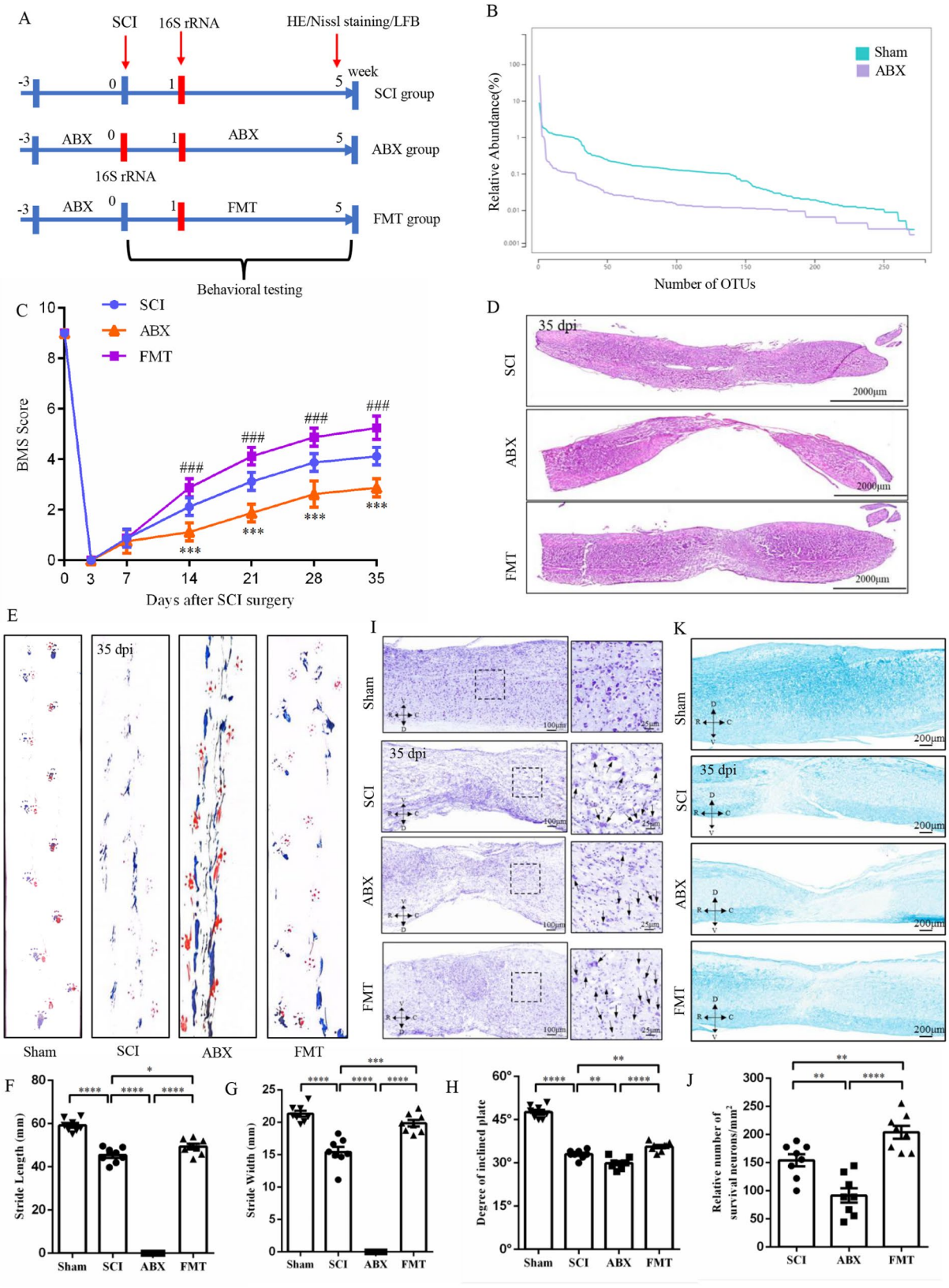

Fig. 2 (See legend on next page.)

(See figure on previous page.)

Fig. 2 FMT treatment promoted functional recovery in mice with SCI. **A**. Experimental scheme diagram. **B**. 16 S rRNA OTUs RANK curve analysis indicated that species expression in ABX group was significantly decreased ($n=10$ per group). **C**. From 14 d.p.i. to the end of observation, the FMT group demonstrated superior recovery outcomes relative to the ABX group. ($n=8$ per group). **D**. Representative images of longitudinal spinal cord sections from multiple experimental groups at 35 d.p.i. stained with HE. Scale bar = 2000 μm. **E**. Representative images of footprint analysis (red for forelimb and blue for hind limbs) in each group at 35 d.p.i. The FMT mice showed moderate step length and stable gait compared with the ABX group. Quantification of the stride length (**F**) and the stride width (**G**) ($n=8$ per group). **H**. Histogram of the Inclined Plane Test showing the maximum angle maintained by mice, with the FMT group exhibiting significant improvement compared to the ABX group ($n=8$ per group). **I**. Representative images of Nissl staining from each group of mice at 35 d.p.i. The images on the right are magnified views of the corresponding areas on the left, with arrows indicating Nissl bodies that represent intact and living neurons. Scale bar = 100 μm; 25 μm for enlarged figures. **J**. Quantification of surviving neurons based on Nissl staining. The FMT group shows significantly improved neuronal survival compared to the SCI and ABX groups. (**K**) Representative images of Luxol Fast Blue staining showing myelin structure in each group at 35 d.p.i., The FMT group showed visibly improved myelin preservation compared to the SCI and ABX groups. Data were presented as Mean ± SEM. For Fig. 2C, ###$P<0.001$ indicates FMT group vs. other two groups; ***$P<0.001$ indicates SCI group vs. ABX group. For other figures, *$P<0.05$, **$P<0.01$, ***$P<0.001$, ****$P<0.0001$

Antibiotic cocktail reduced gut microbiota and FMT enhanced motor recovery

To evaluate the therapeutic effects of FMT on SCI, we first eliminated intestinal flora in ABX and FMT groups with antibiotics for three weeks. Stool samples of ABX-treated mice, collected immediately the antibiotic treatment but before SCI, were compared with those from the sham group using 16 S rRNA sequencing. ABX-treated mice exhibited a decreased relative abundance of taxa and a lower number of operational taxonomic units (OTUs), indicating a significant reduction in microbial diversity (Fig. 2B). α-diversity analyses revealed significant decreases in indices such as Chao1, coverage, Simpson, Observed species, and Shannon (Fig. S1B). PCA, PLS-DA, and NMDS results showed marked variations between sham and ABX-treated mice (Fig. S1C-E). Hierarchical clustering analysis revealed lower relative abundances of families such as *Oscillospiraceae*, *Lachnospiraceae*, and *Muribaculaceae* in the ABX-treated group compared to the sham group. Families like *Desulfovibrionaceae*, *Clostridiaceae1*, and *Rikenellaceae* were present at very low abundances in both groups, but even lower in the ABX group (Fig. S1F). COG analysis indicated significant functional differences due to ABX treatment (Fig. S1G). These findings suggest that the antibiotics regimen effectively reduced gut microbiota composition and diversity.

To further investigate the gut microbiota after FMT, fecal samples from the ABX group at 7 d.p.i. were compared with those from the FMT group using 16 S rRNA analysis. The results demonstrated that the α diversity and β diversity of the FMT group were significantly higher than those of the ABX group at 7 d.p.i. (Fig. S2A, B), indicating that FMT significantly improved the diversity and stability of intestinal flora. PCA, PLS-DA, and NMDS analyses revealed marked differences between the ABX group and FMT group (Fig. S2C-E). At the Genus level, *Enterobacter*, *Parasutterella*, *Parabacteroides*, *Enterococcus*, *Akkermansia*, and *Ligilactobacillus* were significantly more abundant in the FMT group compared to the ABX group (Fig. S2F). At the Phylum level, *Bacteroidota*, *Bacillota*, and *Verrucomicrobiota* were significantly increased, while *Pseudomonadota* was decreased in the FMT group (Fig. S2G). COG functional difference analysis showed that the top 5 enriched functions in the FMT group included RNA processing and modification, Nucleotide transport and metabolism, Signal transduction mechanisms, Intracellular trafficking, secretion and vesicular transport, and Extracellular structures (Fig. S2H). These results suggest that the microbiota composition in the FMT group at 7 d.p.i. more closely resembled that of healthy mice, supporting intestinal microecological balance and positively influencing the spinal cord microenvironment.

In line with the changes in microbial composition, motor function recovery showed that from 14 d.p.i., recovery in the ABX group was markedly diminished compared to the SCI group, while recovery in the FMT group surpassed both the SCI and ABX groups (Fig. 2C). Footprint Analysis revealed significant differences in stride length and stride width across groups. Compared to the sham group, the SCI group exhibited a significantly reduced stride length ($P<0.0001$), indicating impaired motor function following SCI. Notably, the ABX group showed the shortest stride length, suggesting further deterioration of motor coordination and strength in gut microbiota-depleted mice. In contrast, FMT treatment partially restored stride length, which was significantly greater than that observed in the SCI group ($P<0.05$) (Fig. 2F). A similar trend was observed for stride width, where the ABX group displayed the most pronounced deviation, while the FMT group demonstrated significant improvements compared to the SCI group ($P<0.001$) (Fig. 2G). The results of the Inclined Plane Test revealed that the maximum angle at which mice could maintain their position for at least 5 s was 47.63° ± 0.80° in the sham group and significantly decreased to 33.00° ± 0.53° in the SCI group ($P<0.0001$). The ABX group showed a further decline to 29.88° ± 0.69°, indicating greater impairment in motor function. Notably, FMT treatment improved this angle to 35.63° ± 0.56°, which was significantly higher than that of the ABX group ($P<0.0001$), suggesting a partial recovery of motor function and coordination (Fig. 2H).

HE staining at 35 d.p.i. revealed that in the SCI group, the spinal cord structure was intact, with a clearly visible scar at the injury center. In contrast, the ABX group showed atrophied spinal cord tissue and disorganized surrounding tissue structure. The FMT group exhibited relatively edematous spinal cord tissue with a larger scar area than the SCI group (Fig. 2D). Nissl staining was conducted to evaluate neuronal density and structural integrity in the spinal cord across the groups. As shown in Fig. 2I, the sham group displayed abundant intact neuronal cell bodies with clear morphology. In contrast, the SCI group exhibited a significant reduction in neuronal density, with shrunken and irregularly shaped cell bodies. The ABX group showed further exacerbation of neuronal loss. Notably, FMT treatment improved neuronal preservation, as evidenced by increased intact neuronal bodies compared to the SCI and ABX groups. Quantitative analysis (Fig. 2J) confirmed these findings, showing significantly higher neuronal density in the FMT group compared to the SCI group ($P < 0.01$) and the ABX group ($P < 0.0001$). Luxol Fast Blue (LFB) staining results are shown in Fig. 2K, the sham group exhibited dense and uniform blue staining, indicating intact myelin structure. In contrast, the SCI group displayed notable myelin loss, characterized by reduced staining intensity and fragmented architecture. The ABX group showed further deterioration with more disrupted and faint myelin staining. Notably, the FMT group demonstrated improved myelin preservation, with more continuous and intense staining compared to the SCI and ABX groups. These results indicate that ABX treatment reduced gut microflora and aggravated SCI, while FMT treatment promoted spinal cord healing and enhanced motor function recovery.

FMT treatment promoted neural repair

Mice from each group were sacrificed after their final behavioral evaluation. Median sagittal sections, including the lesion center, were prepared and stained with NF-H, a subunit of neurofilaments crucial for axonal regrowth. In the Sham group, NF-H signals were dense and aligned parallel to the longitudinal axis, indicating robust axonal integrity. The ABX mice displayed a substantial region devoid of NF-H staining, suggesting severe axonal damage (Fig. 3A). Quantification of NF-H intensity among the four groups was shown in Fig. 3B. Neuronal survival following FMT treatment was assessed by immunostaining for NeuN and activated caspase-3 at 14 d.p.i., the ABX group exhibited a significantly greater percentage of aCaspase-3+/NeuN + cells than the SCI group ($P = 0.009$), indicating enhanced neuronal apoptosis. FMT treatment substantially reduced the proportion of aCaspase-3+/NeuN + cells compared to the ABX group, suggesting improved neuronal survival. These findings indicate that FMT treatment promoted neural integrity and supported axonal regeneration following SCI (Fig. 3C, D).

FMT treatment reduced glia scar formation and inhibited inflammation infiltration

Astrocytic gliosis and the inflammation are critical factors affecting spinal cord function following injury. Astrocyte and immune cell activation was examined by IF staining with GFAP, IBA1, and CD68 at 14 d.p.i. As shown in Fig. 4A, after SCI, IBA1 + activated macrophages/microglia clustered in the lesion center and were surrounded by activated astrocytes (GFAP+). In the ABX group, the lesion area was significantly expanded, with extensively infiltration of IBA1 + immune cells around the injury center and multiple foci of glial hyperplasia within the injury center (indicated by the white dashed line). FMT resulted in a marked reduction in the size of the glial scar and the number of lesion compartments (Fig. 4B, C). Enlarged images revealed inflammatory cells crossing the glial boundary into the injured parenchyma.

A detailed analysis of the spatial distribution pattern of the phagocytic marker CD68 in the region of interest was performed using ImageJ. In the SCI group, CD68 + signals were predominantly localized to the injury center, with a gradual decrease in intensity towards the periphery. In contrast, the ABX group showed markedly lower CD68 expression at the injury center, with increase expression in the periphery regions. The FMT treatment group exhibited a more uniform distribution of CD68 across the lesion site (Fig. 4D). These findings suggest that FMT treatment significantly modified the spatial distribution of CD68 + cells, potentially indicating a more regulated and less extensive inflammatory response in the spinal cord.

FMT treatment alleviated extracellular matrix (ECM) compaction

Matrix compacting plays a crucial role in spinal cord wound healing [22, 23]. We examined the extracellular matrix proteins fibronectin and collagen I at 14 d.p.i. to evaluate the impact of FMT on matrix expression following injury. The expression of these matrix proteins was minimal in the uninjured spinal cord but significantly upregulated after injury (Fig. 5A, C). In the SCI group, collagen I and fibronectin were compacted in the lesion center, surrounded by a reactive astrocytic scar. Conversely, in the ABX group, fibronectin expression appeared widespread. Quantification of the lesion area indicated by fibronectin, and collagen I showed a significant reduction following FMT treatment (Fig. 5B, D).

Vascular rearrangement and repair are pivotal during spinal cord wound healing. A recent study reported that FMT treatment significantly increased blood vessel fragmentation in SCI mice [24]. In our study, the expression

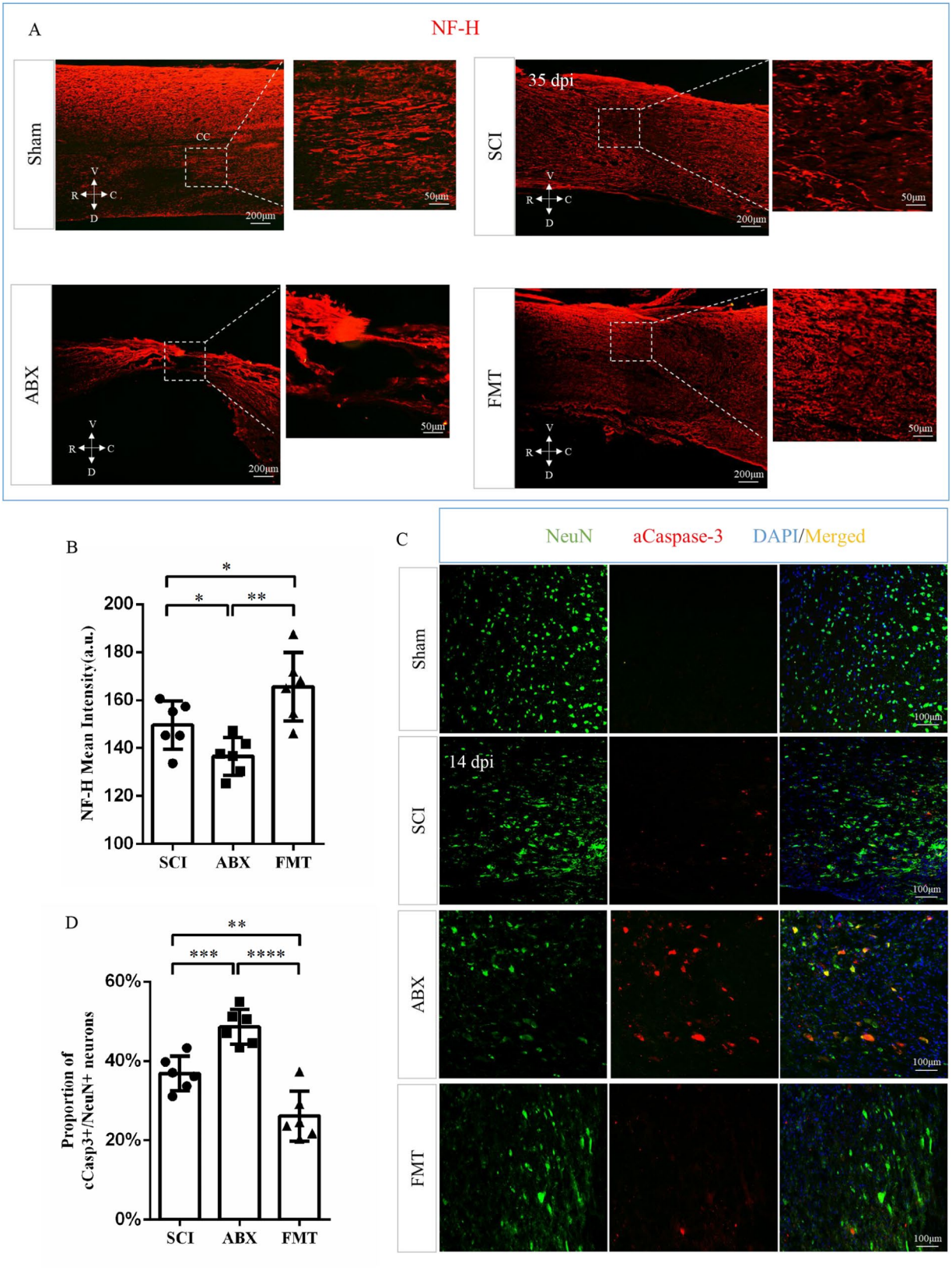

Fig. 3 (See legend on next page.)

(See figure on previous page.)

Fig. 3 FMT treatment promoted axonal regeneration and neuronal survival. **A**. Representative images of NF-H staining in each group. Scale bar = 200 μm; 50 μm for enlarged figures. **B**. Quantification of NF-H staining intensity in different experimental groups ($n = 6$ per group). **C**. IF staining for NeuN (green) and activated caspase-3 (red) in the central sagittal section of the spinal cord. Scale bar = 100 μm.**D**. Quantification of cells co-staining for NeuN and activated caspase-3 (aCasp3) ($n = 6$ per group). Data were presented as Mean ± SEM. *$P < 0.05$, **$P < 0.01$, ***$P < 0.001$, ****$P < 0.0001$. cc: central canal; R: rostral; C: caudal; D: dorsal; V: ventral; dpi: day post injury

of endothelial marker PECAM-1 was evaluated. We observed that PECAM-1 expression intensity was comparable among the four groups (Fig. 5E, F) ($P > 0.05$). In the ABX mice, neurovascular structures at the lesion site showed engorgement with large lumen size, whereas in the FMT-treated mice, the lumen size returned to the levels observed in the SCI group (Fig. 5G). Additionally, blood vessels in the SCI group exhibited a well-aligned pattern, while those in the ABX group showed a random orientation (Fig. 5H).

FMT regulated transcriptional modifications in spinal cord tissue

To comprehensively assess mRNA expression patterns following FMT, spinal cord tissue was extracted from each experimental group for RNA sequencing analysis at 7 d.p.i. Compared to the sham mice, the SCI mice showed 4636 differentially expressed genes (DEGs), comprising 2737 up-regulated and 1899 down-regulated genes (Fig. 6A, B). Following microbiota depletion in ABX group, 245 DEGs were identified relative to the SCI group, with142 genes showing increased expression, and 103 genes showing decreased expression. FMT treatment resulted in a distinct gene expression profile compared to the ABX mice, with 393 DEGs observed, including 183 genes with increased expression and 210 genes with decreased expression. The top 20 DEGs in each group were further analysed using gene heat mapping, depicted in Fig. 6C. Notably, the up-regulated and down-regulated DEGs in the ABX group exhibited reversed expression patterns in the FMT group. KEGG analysis revealed that the ABX group had a predominant upregulation of biological processes associated with cytokine interactions, substance metabolism, and inflammation compared to the SCI group (Fig. 6D). Interestingly, FMT treatment led to the enrichment of biological processes related to material metabolism, extracellular matrix deposition, and anti-inflammatory responses following the restoration of intestinal flora in mice (Fig. 6E). These findings highlight the potential of FMT to modulate these pathways beneficially in the context of SCI. GO analysis of DEGs results were provided in Fig. S4.

Discussion

Spinal cord injury (SCI) represents a formidable challenge in the treatment of central nervous system (CNS) disorders, characterized by a high incidence rate and significant therapeutic difficulties [25, 26]. Emerging research suggests that imbalances in gut microbial communities might influence the pathogenesis and functional recovery of SCI [5, 6, 27]. The findings of this study provide compelling evidence that fecal microbiota transplantation (FMT) can significantly improve motor function recovery in mice with SCI. By restoring gut microbiota balance, FMT influences the spinal microenvironment, promoting neuronal survival, axonal regeneration, alleviating extra cellular matrix (ECM) deposition and reducing neuroinflammation.

The disruption of gut microbiota following SCI is well-documented, with dysbiosis contributing to exacerbated injury and impaired recovery [28–30]. Previous research has shown significant differences in microbial diversity indices like Chao1, observed species, Shannon, and Simpson indexes between SCI and sham groups [9]. Our findings showed significant differences only in the Chao1 and coverage indices. Interestingly, our results also revealed downward trends in the Shannon, Simpson, and Ace indices, but these did not reach statistical significance. This discrepancy may stem from the distinct diversity components captured by these indices. Chao1 and coverage indices focus on species richness and are particularly sensitive to rare taxa, which may be disproportionately affected by SCI. In contrast, Shannon, Simpson, and Ace incorporate both richness and evenness, making them less responsive to changes predominantly involving rare species [31, 32]. These subtle shifts may require larger sample sizes or deeper sequencing to achieve statistical significance. Furthermore, Environmental factors such as diet, SCI severity, and methodological differences could also explain the variability in findings [33, 34]. Future studies integrating multi-omics approaches could shed more light on deepening functional understanding of microbial communities in SCI. FMT from healthy donors successfully restored the gut microbiota balance, aligning with previous studies that have demonstrated the beneficial effects of FMT in restoring microbiota balance in various conditions [35, 36]. In line with the restoring of gut microbiota, behavioral assessments showed significant improvements in motor function in FMT-treated mice compared with the SCI group from 14 d.p.i. to the end of observation period. The findings indicate that the SCI-induced imbalance of the gut microbiome is significantly alleviated by FMT treatment, which promotes motor recovery.

Motor function recovery after SCI depends on the survival of neurons and the extension of axons to their

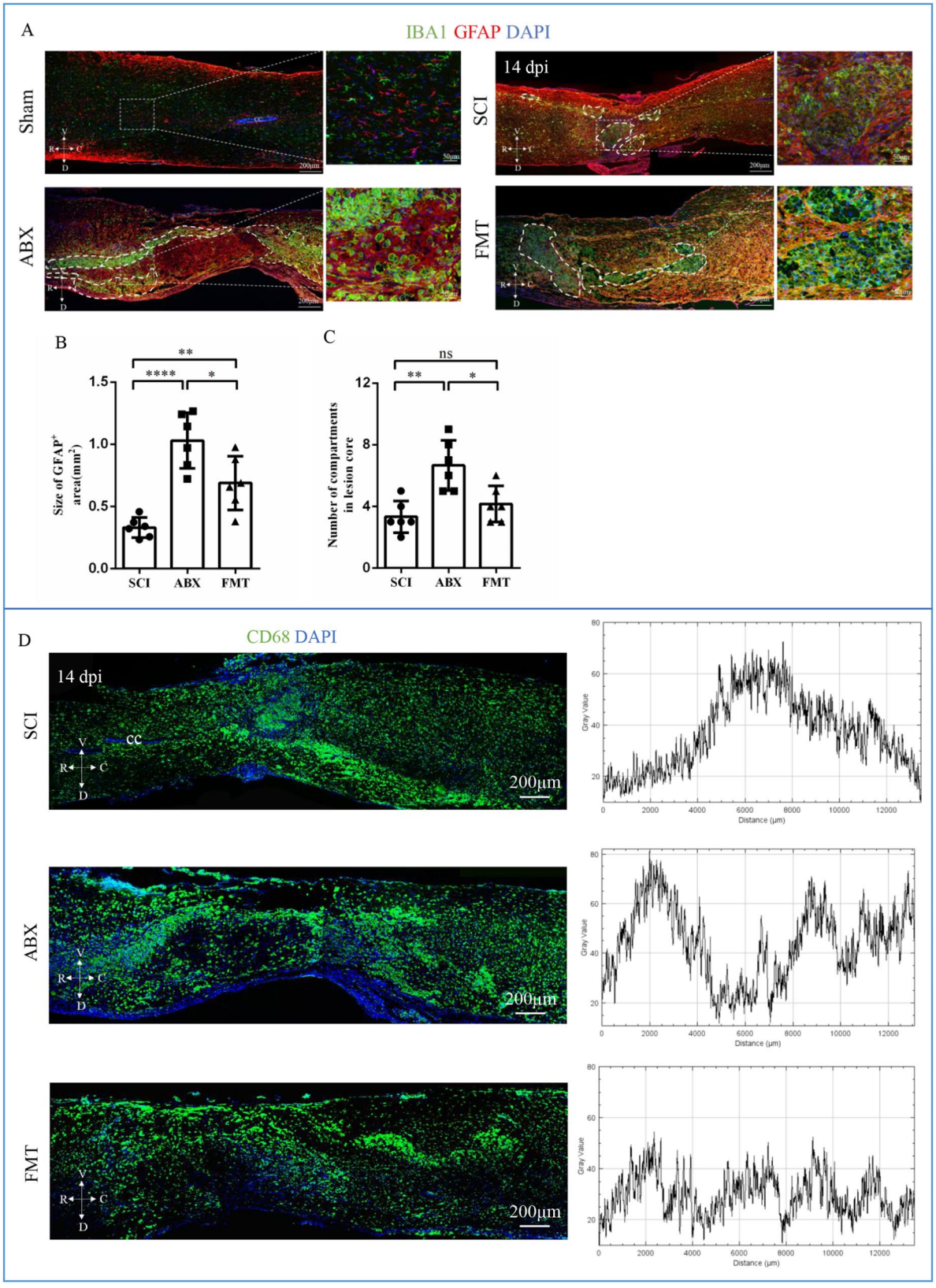

Fig. 4 (See legend on next page.)

(See figure on previous page.)

Fig. 4 FMT treatment diminished glial scarring and mitigated inflammation. **A**. Representative images of IBA1 and GFAP staining are shown. In the SCI group, IBA1 + cells aggregated within the lesion center. The ABX group displayed a significant expansion of the lesion cavity, with extensive infiltration of IBA1 + cells around the injury center and multiple glial hyperplasia foci within the injury site. Enlarged images revealed that, in the SCI group, IBA1 + cells were predominantly constrained by astrocytic borders, whereas in the ABX group, many IBA1 + cells crossed the scar boundary and infiltrated the injury periphery. Scale bar = 200 μm; 50 μm for enlarged figures. **B**. Quantification of the GFAP + area size ($n = 6$ per group). (**C**) Quantification of the number of glial hyperplasia foci ($n = 6$ per group). (**D**) Representative images of CD68 staining in each group (left) and corresponding fluorescence intensity spectra (right). Scale bar = 200 μm. Data were presented as Mean ± SEM. *$P < 0.05$, **$P < 0.01$, ****$P < 0.0001$, ns = No significance. cc: central canal; R: rostral; C: caudal; D: dorsal; V: ventral; dpi: day post injury

specific targets [37]. We observed that FMT-treated mice exhibited remarkable enhancement in neuronal survival and axonal regeneration compared to controls. Immunofluorescence staining revealed increased neuronal survival and reduced apoptotic neurons in the FMT-treated group. These results align with previous studies suggesting that FMT promotes neuroplasticity [38, 39]. To determine if FMT treatment affects cell proliferation after SCI, we conducted IF staining using the proliferation marker Ki67. Our analysis revealed that the number of Ki67 + cells remained comparable across all groups (Fig. S3). This finding suggests that the functional recovery observed is likely not due to increased cell proliferation. The enhanced axonal regeneration observed in our study supports the hypothesis that gut microbiota can influence neural repair processes.

Neuroinflammation, characterized by complex interactions between immune cells and glial cells such as macrophages/microglia and astrocytes, can either facilitate tissue repair or worsen secondary injury [40, 41]. In our study, SCI mice treated with FMT exhibited a distinct pattern of immune cell distribution compared to ABX mice. Specifically, IBA1 + activated macrophages/microglia clustered centrally encircled by astrocytic scar, indicating a controlled inflammatory response. In contrast, ABX mice showed expanded lesion areas with extensive infiltration of IBA1 + cells and multiple glial hyperplasia foci. Distribution of CD68 + phagocytic cells indicated distinct inflammatory patterns among groups. In the SCI mice, CD68 + cells were mainly concentrated at the injury center. The ABX group showed reduced CD68 at the center with increased presence in peripheral areas, suggesting altered inflammation due to antibiotics. The FMT group exhibited a more even distribution of CD68, indicating a balanced immune response and potentially enhanced tissue repair. Our results align with previous studies that emphasize microbiota's impact on modulating neuroinflammation and providing neuroprotection following SCI [15, 16, 42]. The observed compact ECM deposition, including collagen I and fibronectin, in the SCI lesion center underscores their role in creating a dense tissue that can promote wound repair and healing [23, 43]. The widespread expression of fibronectin in the ABX group and its reduction in the FMT treatment group suggests that FMT may attenuate detrimental ECM remodeling, facilitating a more conducive environment for healing. Though PECAM-1 expression levels were similar across groups, indicating consistent vascular density, the neurovascular organization altered markedly. The ABX group exhibited enlarged blood vessels with disrupted integrity, whereas the FMT group showed normalized vessel size and better-aligned vasculature. These improvements in vascular architecture likely enhance nutrient and oxygen delivery, which is crucial for spinal cord repair and functional recover [44]. The reduction of ECM deposition and glial scar formation observed in FMT-treated mice highlights its therapeutic potential for human SCI patients. Excessive ECM deposition is a well-recognized barrier to axonal regeneration, and therapies targeting ECM remodeling could be combined with existing regenerative strategies, such as stem cell transplantation or biomaterials, to enhance recovery [45–48]. Furthermore, FMT's anti-inflammatory properties could mitigate secondary injury, providing a dual benefit for neural repair.

Prolonged antibiotic treatment in the ABX and FMT groups was employed to deplete gut microbiota, creating a baseline for evaluating the effects of FMT. However, antibiotics are known to induce significant changes beyond microbiota depletion, including increased gut permeability, altered immune responses, and potential systemic effects, which may influence the spinal microenvironment [49, 50]. These effects could contribute to inflammatory modulation and ECM remodeling observed in the study. While FMT partially restores the gut microbiota, future studies should investigate the specific contributions of antibiotics to gut-spinal axis interactions and SCI outcomes.

To delve into the molecular underpinnings of FMT's therapeutic potential, we utilized RNA sequencing analysis to explore the intricate gene expression changes following SCI and to evaluate how FMT influenced these patterns. Our RNA sequencing analysis identified substantial variations in gene expression across groups. In the SCI group, we identified 4636 differentially expressed genes (DEGs) compared to the sham group, with a substantial number of genes being either up-regulated or down-regulated, indicating a robust inflammatory and metabolic response to injury. The ABX group showed 245 DEGs relative to the SCI group, with notable changes in cytokine interactions and inflammatory pathways. Interestingly, FMT treatment led to 393 DEGs compared to the ABX group, suggesting a shift

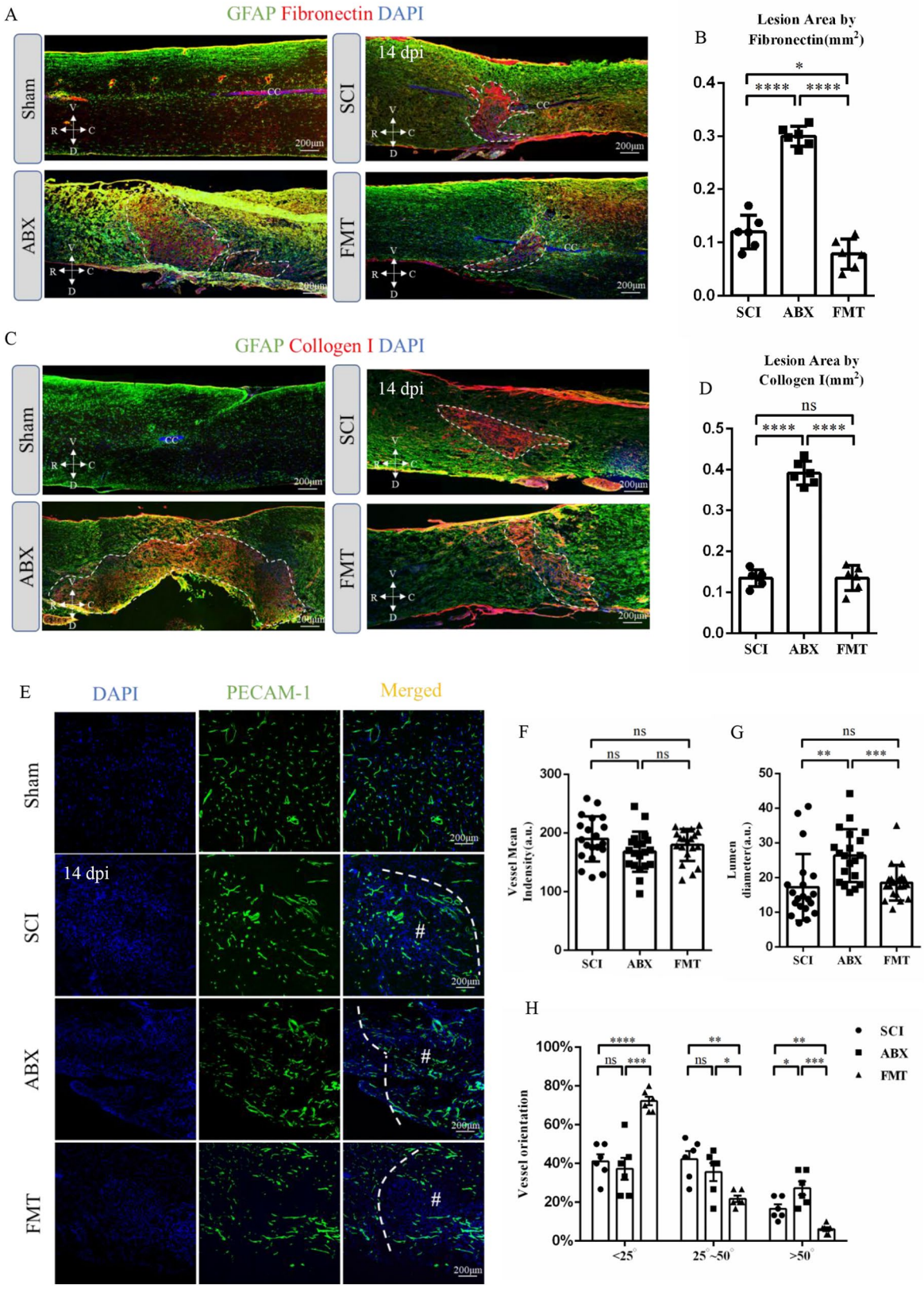

Fig. 5 (See legend on next page.)

(See figure on previous page.)

Fig. 5 FMT treatment promoted ECM constriction and modulated neurovascular expression Patterns. **A**. Typical images of double staining for GFAP and Fibronectin. Scale bar = 200 μm. **B**. Quantification of lesion areas marked by Fibronectin staining ($n = 6$ per group). **C**. Typical images of sagittal spinal cord sections from different groups, double-stained for GFAP and Collagen I. Scale bar = 200 μm. **D**. Quantification of lesion areas marked by Collagen I staining ($n = 6$ per group). **E**. Typical images of PECAM-1 staining. Scale bar = 200 μm. **F**. Statistical analysis of mean fluorescence intensity for PECAM-1 showing no significant differences among groups ($n = 6$ per group). **G**. Quantification of lumen diameter ($n = 6$ per group). H. Quantification of PECAM-1 positive blood vessel orientation. The ABX group exhibited a significant increase in large-angle (> 50°) blood vessels in comparison with the SCI group. FMT markedly elevated the proportion of small-angle (< 25°) vessels while reducing the proportions of large-angle (> 50°) and medium-angle (25°-50°) vessels ($n = 6$ per group). Data were presented as Mean ± SEM. *$P < 0.05$, **$P < 0.01$, ***$P < 0.001$, ****$P < 0.0001$, ns = No significance. cc: central canal; R: rostral; C: caudal; D: dorsal; V: ventral; dpi: day post injury

towards gene expression profiles associated with material metabolism, extracellular matrix deposition, and anti-inflammatory responses. KEGG analysis of these DEGs revealed that the activated genes at 7 d.p.i. were involved in inflammation regulation, extracellular matrix (ECM) remodeling, and neuroprotection. Notably, the cytokine-cytokine receptor interaction pathway, the top differentially expressed pathway between the FMT and ABX groups, plays a key role in immune responses and inflammation [51]. This upregulation may help reduce glial scar formation and inflammation, both of which hinder recovery after SCI. Additionally, the downregulation of Col28a1 expression in the FMT group suggests that restoring ECM-receptor interaction integrity could promote axon regeneration by preventing inhibitory barriers [52]. Furthermore, pathways related to neurovascular remodeling, such as the HIF-1 signaling pathway, which can upregulate the expression of various pro-angiogenic genes like VEGF, were upregulated in FMT-treated mice, potentially enhancing blood-brain barrier integrity and nutrient supply to the spinal cord [53]. The PI3K-AKT signaling pathway, involved in neurogenesis, was also activated, supporting neural regeneration and motor function recovery [54]. These findings suggest that FMT treatment induces molecular changes that may facilitate tissue repair and recovery following SCI.

While previous studies have demonstrated the therapeutic potential of FMT in spinal SCI [9, 16, 17, 24], our study provides new insights into the broader mechanisms by which FMT promotes functional recovery. FMT has been shown to modulate the microbiota-gut-spinal cord axis, regulate immune responses, and improve spinal cord pathology. However, our findings offer additional perspectives by focusing on the restoration of gut microbiota diversity and its direct link to motor function recovery post-SCI. Notably, our study highlights how FMT affects not only immune cell regulation but also the structural environment at the injury site, including extracellular matrix remodeling and neuroinflammation. This broader view helps to explain the improvements in both spinal cord tissue integrity and functional outcomes observed in FMT-treated mice. Additionally, while previous studies have identified shifts in microbial populations and their association with functional recovery, our work emphasizes the critical role of restoring gut microbiota diversity. We found that the restoration of microbial balance correlated with improved motor function and a more favorable microenvironment for tissue repair, further supporting the potential of FMT as an effective treatment strategy for SCI. Taken together, our study provides a more comprehensive understanding of how FMT can influence spinal cord regeneration by addressing both immune and structural components of SCI, offering a promising therapeutic approach with broad implications for future SCI treatments.

Conclusions

In summary, our study demonstrates that FMT effectively modifies the spinal microenvironment, leading to improved motor function recovery in mice with SCI. By restoring gut microbiota balance, reducing neuroinflammation, and enhancing ECM remodeling, FMT fosters an environment conducive to neural repair and functional recovery. This study highlights FMT's potential in treating SCI and underscores the need for further research to translate these insights into clinical applications.

Figure S1. ABX significantly reduced gut microbiota composition and diversity. A. α diversity indices (Chao, Ace, Coverage, Simpson, Observed species, Shannon) and β diversity index (B) comparing the Sham and ABX-treated mice. C. Principal Component Analysis (PCA) between the Sham and ABX-treated groups. D. PLS-DA plot demonstrating a clear distinction between the Sham and ABX-treated mice. E. NMDS plot revealing distinct clustering, with Sham and ABX-treated groups occupying distinct regions in the ordination space. F. Hierarchical clustering analysis of microbial community composition in Sham and ABX-treated groups. G. Clusters of Orthologous Groups (COG) function analysis of the Sham and ABX-treated group.

Figure S2. FMT significantly restored the composition and diversity of gut microbiota. (A) α-Diversity indices (Shannon, Simpson, and Coverage) comparing the ABX and FMT-treated groups at 7 d.p.i. (B) β-Diversity index showing differences in microbial composition between the ABX and FMT-treated groups at 7 d.p.i. (C) Principal Component Analysis (PCA) showing distinct microbial community structures between the ABX and FMT groups. (D) Partial Least Squares Discriminant Analysis (PLS-DA) plot demonstrating clear separation between

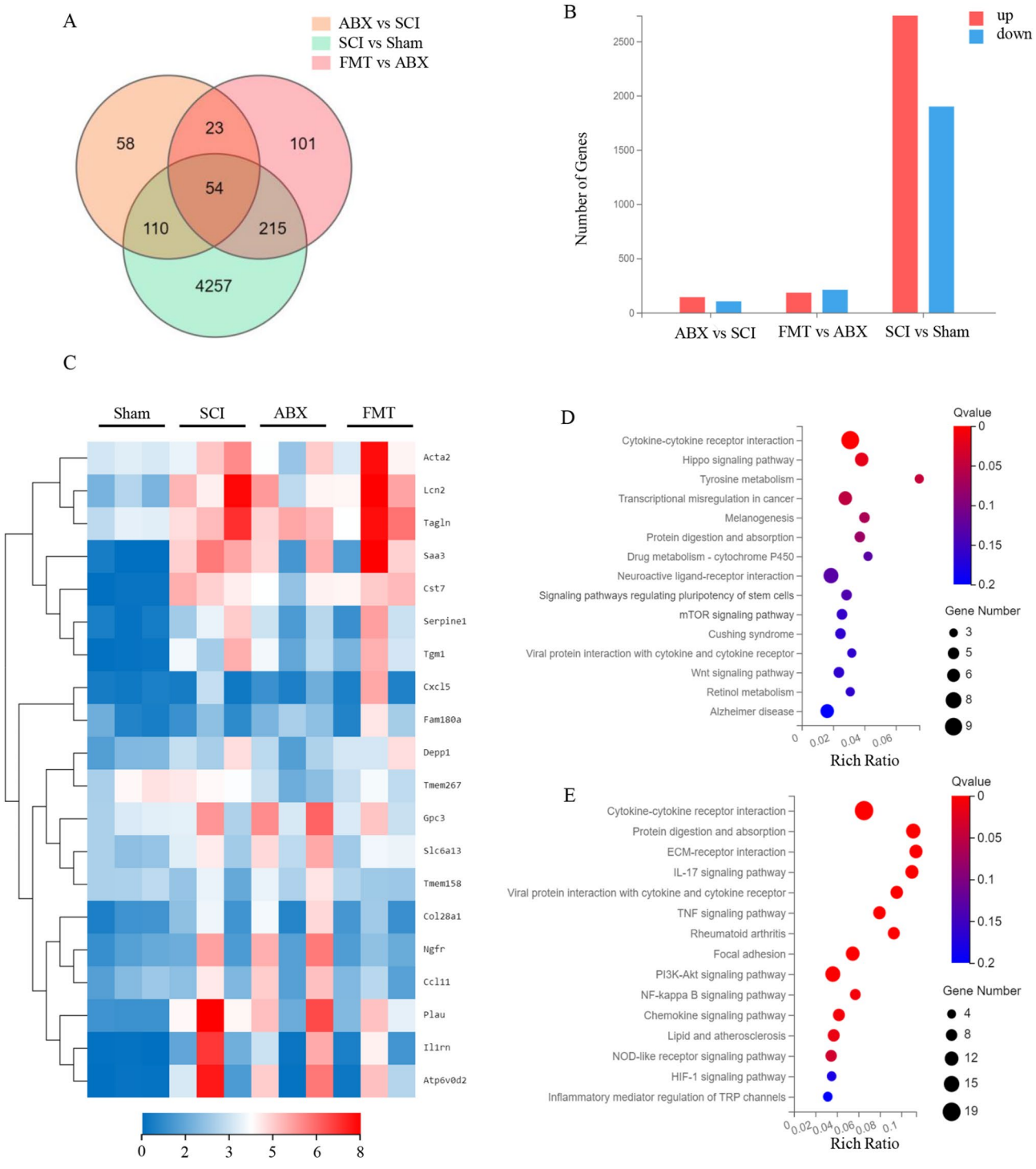

Fig. 6 Modulation of spinal cord tissue transcriptome by FMT treatment. **A**. Differentially expressed genes (DEGs) across each group are displayed using a Venn diagram. **B**. The number of DEGs that are upregulated and downregulated between the groups is depicted in a histogram. **C**. Heatmap analysis of the top 20 DEGs in each group, demonstrating that FMT treatment reversed many DEGs in the ABX group. KEGG pathway enrichment analysis shows pathways upregulated in the ABX group relative to the SCI group (**D**) and pathways upregulated in the FMT group compared to the ABX group (**E**) ($n = 3$ per group, fold change > 1.5)

the ABX and FMT groups. (E) Non-metric multidimensional scaling (NMDS) plot revealing distinct clustering, with ABX and FMT groups occupying separate regions in the ordination space. (F) Hierarchical clustering analysis of microbial community composition at the genus level in ABX and FMT groups at 7 d.p.i. (G) Hierarchical clustering analysis at the phylum level comparing microbial composition between ABX and FMT groups. (H) Clusters of Orthologous Groups (COG) functional analysis comparing the gut microbiota in ABX and FMT-treated groups at 7 d.p.i.

Figure S3. Effects of FMT treatment on cell proliferation. (A) IF staining showing representative images of Ki67 + proliferating cells in each group. Scale bar = 200 μm. (B) Quantitative analysis of Ki67 + cells across groups, indicating similar levels of proliferating cells among the SCI, ABX, and FMT groups ($n = 6$ per group). Data were presented as Mean ± SEM. $^{****}P < 0.0001$, ns = No significance.

Figure S4. Analysis of differentially expressed genes (DEGs) using Gene Ontology (GO).

(A) The top 20 enriched biological processes identified by GO analysis in the ABX group in comparison with the SCI group. (B) The top 20 enriched biological processes identified by GO analysis in the FMT group in comparison with the ABX group. This analysis highlights the biological processes most affected by antibiotic treatment and FMT in SCI.

Abbreviations

SCI	Spinal cord injury
FMT	Fecal microbiota transplantation
ABX	antibiotic cocktail
RNA-seq	RNA sequencing
ECM	Extracellular matrix
CNS	Central nervous system
SCFAs	Short-chain fatty acids
BMS	Basso Mouse Scale
OTUS	Operational taxonomic units
PCA	Principal Component Analysis
PLS-DA	Partial Least Squares Discriminant Analysis
NMDS	Non-metric multidimensional scaling
COG	Clusters of Orthologous Groups
DEGs	Differentially expressed genes
GO	Gene Ontology
KEGG	Kyoto Encyclopedia of Genes and Genomes
HE	Hematoxylin-Eosin
PFA	Paraformaldehyde
OCT	Optimal cutting temperature compound
NF-H	Neurofilament heavy polypeptide
GFAP	Glial fibrillary acidic protein
IBA1	Ionized calcium binding adaptor molecule 1
aCaspase-3	Activated caspase-3
DAPI	Diamidinyl phenyl indole
IL-17	Interleukin-17
PBS	Phosphate buffered saline
SEM	Standard Error of the Mean
ANOVA	Analysis of variance
NeuN	Neuronal nuclear protein
PECAM-1	Platelet endothelial cell adhesion molecule-1
d.p.i.	Days post-injury
LFB	Luxol Fast Blue

Supplementary Information

The online version contains supplementary material available at https://doi.org/10.1186/s12967-025-06232-9.

Supplementary Material 1: Fig. S1. ABX significantly reduced gut microbiota composition and diversity.A. α diversity indices (Chao, Ace, Coverage, Simpson, Observed species, Shannon) and β diversity index (B) comparing the Sham and ABX-treated mice. C. Principal Component Analysis (PCA) between the Sham and ABX-treated groups. D. PLS-DA plot demonstrating a clear distinction between the Sham and ABX-treated mice. E. NMDS plot revealing distinct clustering, with Sham and ABX-treated groups occupying distinct regions in the ordination space. F. Hierarchical clustering analysis of microbial community composition in Sham and ABX-treated groups. G. Clusters of Orthologous Groups (COG) function analysis of the Sham and ABX-treated group.

Supplementary Material 2: Fig. S2. FMT significantly restored the composition and diversity of gut microbiota.(A) α-Diversity indices (Shannon, Simpson, and Coverage) comparing the ABX and FMT-treated groups at 7 d.p.i. (B) β-Diversity index showing differences in microbial composition between the ABX and FMT-treated groups at 7 d.p.i. (C) Principal Component Analysis (PCA) showing distinct microbial community structures between the ABX and FMT groups. (D) Partial Least Squares Discriminant Analysis (PLS-DA) plot demonstrating clear separation between the ABX and FMT groups. (E) Non-metric multidimensional scaling (NMDS) plot revealing distinct clustering, with ABX and FMT groups occupying separate regions in the ordination space. (F) Hierarchical clustering analysis of microbial community composition at the genus level in ABX and FMT groups at 7 d.p.i. (G) Hierarchical clustering analysis at the phylum level comparing microbial composition between ABX and FMT groups. (H) Clusters of Orthologous Groups (COG) functional analysis comparing the gut microbiota in ABX and FMT-treated groups at 7 d.p.i.

Supplementary Material 3: Fig. S3. Effects of FMT treatment on cell proliferation.A. IF staining showing representative images of Ki67+ proliferating cells in each group. Scale bar=200μm. B. Quantitative analysis of Ki67+ cells across groups, indicating similar levels of proliferating cells among the SCI, ABX, and FMT groups (n=6 per group). Data were presented as Mean ± SEM. ****P < 0.0001, ns=No significance.

Supplementary Material 4: Fig. S4. Analysis of differentially expressed genes (DEGs) using Gene Ontology (GO).A. The top 20 enriched biological processes identified by GO analysis in the ABX group in comparison with the SCI group. B. The top 20 enriched biological processes identified by GO analysis in the FMT group in comparison with the ABX group. This analysis highlights the biological processes most affected by antibiotic treatment and FMT in SCI.

Supplementary Material 5

Acknowledgements
Not applicable.

Author contributions
Conceptualization: ZLZ and ZZL; animal model establishment: HX, LYZ, QXH; Experiment implementation: JJC, SY; Supervision: ZLZ; Formal analysis: HZ. Writing and editing: ZLZ, HX. All authors read and approved the final manuscript.

Funding
This work was supported by Science and Technology Project Foundation of Guangzhou City (Grant number 202201010803 to ZLZ) and Science and Technology Project Foundation of Guangzhou City (Grant number 2024A03J1068 to HZ).

Data availability
The datasets used and/or analyzed during the current study are available from. the corresponding author on reasonable request.

Declarations

Ethics approval and consent to participate
Experiments were carried out according to the National Institutes of Health Guide for the Care and Use of Laboratory Animals (8th edition, 2011) and all procedures were approved by the Institutional Animal Care and Use Committee of Guangdong Second Provincial General Hospital (approval No. 2023-DW-KZ-091-01).

Consent for publication
Not applicable.

Competing interests
The authors declare that they have no competing interests.

Author details
[1]The First Affiliated Hospital of Jinan University, Guangzhou, Guangdong Province 510630, China
[2]The Affiliated Guangdong Second Provincial General Hospital of Jinan University, Guangzhou, Guangdong Province 510317, China

Received: 24 July 2024 / Accepted: 11 February 2025
Published online: 20 February 2025

References

1. Khaing ZZ, Chen JY, Safarians G, Ezubeik S, Pedroncelli N, Duquette RD, Prasse T, Seidlits SK. Clinical trials targeting secondary damage after traumatic spinal cord Injury. Int J Mol Sci. 2023;24:3824.
2. O'Shea TM, Burda JE, Sofroniew MV. Cell biology of spinal cord injury and repair. J Clin Invest. 2017;127:3259–70.
3. Belkaid Y, Hand TW. Role of the microbiota in immunity and inflammation. Cell. 2014;157:121–41.
4. Wang Q, Yang Q, Liu X. The microbiota-gut-brain axis and neurodevelopmental disorders. Protein Cell. 2023;14:762–75.
5. He N, Shen G, Jin X, Li H, Wang J, Xu L, Chen J, Cao X, Fu C, Shi D, et al. Resveratrol suppresses microglial activation and promotes functional recovery of traumatic spinal cord via improving intestinal microbiota. Pharmacol Res. 2022;183:106377.
6. Jing Y, Yang D, Bai F, Wang Q, Zhang C, Yan Y, Li Z, Li Y, Chen Z, Li J, Yu Y. Spinal cord injury-induced gut dysbiosis influences neurological recovery partly through short-chain fatty acids. NPJ Biofilms Microbiomes. 2023;9:99.
7. Li Z, Xiong W, Liang Z, Wang J, Zeng Z, Kołat D, Li X, Zhou D, Xu X, Zhao L. Critical role of the gut microbiota in immune responses and cancer immunotherapy. J Hematol Oncol. 2024;17:33.
8. Su X, Gao Y, Yang R. Gut microbiota derived bile acid metabolites maintain the homeostasis of gut and systemic immunity. Front Immunol. 2023;14:1127743.
9. Kang JN, Sun ZF, Li XY, Zhang XD, Jin ZX, Zhang C, Zhang Y, Wang HY, Huang NN, Jiang JH, Ning B. Alterations in gut microbiota are related to metabolite profiles in spinal cord injury. Neural Regen Res. 2023;18:1076–83.
10. Kong G, Zhang W, Zhang S, Chen J, He K, Zhang C, Yuan X, Xie B. The gut microbiota and metabolite profiles are altered in patients with spinal cord injury. Mol Brain. 2023;16:26.
11. Zhang C, Zhang W, Zhang J, Jing Y, Yang M, Du L, Gao F, Gong H, Chen L, Li J, et al. Gut microbiota dysbiosis in male patients with chronic traumatic complete spinal cord injury. J Transl Med. 2018;16:353.
12. Chen R, Xu Y, Wu P, Zhou H, Lasanajak Y, Fang Y, Tang L, Ye L, Li X, Cai Z, Zhao J. Transplantation of fecal microbiota rich in short chain fatty acids and butyric acid treat cerebral ischemic stroke by regulating gut microbiota. Pharmacol Res. 2019;148:104403.
13. Kim MS, Kim Y, Choi H, Kim W, Park S, Lee D, Kim DK, Kim HJ, Choi H, Hyun DW, et al. Transfer of a healthy microbiota reduces amyloid and tau pathology in an Alzheimer's disease animal model. Gut. 2020;69:283–94.
14. Sun J, Xu J, Ling Y, Wang F, Gong T, Yang C, Ye S, Ye K, Wei D, Song Z, et al. Fecal microbiota transplantation alleviated Alzheimer's disease-like pathogenesis in APP/PS1 transgenic mice. Transl Psychiatry. 2019;9:189.
15. Zhao Z, Ning J, Bao XQ, Shang M, Ma J, Li G, Zhang D. Fecal microbiota transplantation protects rotenone-induced Parkinson's disease mice via suppressing inflammation mediated by the lipopolysaccharide-TLR4 signaling pathway through the microbiota-gut-brain axis. Microbiome. 2021;9:226.
16. Jing Y, Yu Y, Bai F, Wang L, Yang D, Zhang C, Qin C, Yang M, Zhang D, Zhu Y, et al. Effect of fecal microbiota transplantation on neurological restoration in a spinal cord injury mouse model: involvement of brain-gut axis. Microbiome. 2021;9:59.
17. Xi D, Liu P, Feng Y, Teng Y, Liang Y, Zhou J, Deng H, Zeng G, Zong S. Fecal microbiota transplantation regulates the microbiota-gut-spinal cord axis to promote recovery after spinal cord injury. Int Immunopharmacol. 2024;126:111212.
18. Li Y, He X, Kawaguchi R, Zhang Y, Wang Q, Monavarfeshani A, Yang Z, Chen B, Shi Z, Meng H, et al. Microglia-organized scar-free spinal cord repair in neonatal mice. Nature. 2020;587:613–8.
19. Dias DO, Kim H, Holl D, Werne Solnestam B, Lundeberg J, Carlén M, Göritz C, Frisén J. Reducing pericyte-derived scarring promotes recovery after spinal cord Injury. Cell. 2018;173:153–e165122.
20. Fu H, Zhao Y, Hu D, Wang S, Yu T, Zhang L. Depletion of microglia exacerbates injury and impairs function recovery after spinal cord injury in mice. Cell Death Dis. 2020;11:528.
21. Hu Y, Zhang X, Zhang J, Xia X, Li H, Qiu C, Liao Y, Chen H, He Z, Song Z, Zhou W. Activated STAT3 signaling pathway by ligature-induced periodontitis could contribute to neuroinflammation and cognitive impairment in rats. J Neuroinflammation. 2021;18:80.
22. Bradbury EJ, Burnside ER. Moving beyond the glial scar for spinal cord repair. Nat Commun. 2019;10:3879.
23. Zhou X, Wahane S, Friedl MS, Kluge M, Friedel CC, Avrampou K, Zachariou V, Guo L, Zhang B, He X, et al. Microglia and macrophages promote corralling, wound compaction and recovery after spinal cord injury via Plexin-B2. Nat Neurosci. 2020;23:337–50.
24. Jing Y, Bai F, Wang L, Yang D, Yan Y, Wang Q, Zhu Y, Yu Y, Chen Z. Fecal microbiota transplantation exerts neuroprotective effects in a mouse spinal cord Injury Model by modulating the Microenvironment at the Lesion Site. Microbiol Spectr. 2022;10:e0017722.
25. Courtine G, Sofroniew MV. Spinal cord repair: advances in biology and technology. Nat Med. 2019;25:898–908.
26. Ding W, Hu S, Wang P, Kang H, Peng R, Dong Y, Li F. Spinal cord Injury: The Global incidence, prevalence, and disability from the global burden of Disease Study 2019. Spine (Phila Pa 1976). 2022;47:1532–40.
27. Kigerl KA, Hall JC, Wang L, Mo X, Yu Z, Popovich PG. Gut dysbiosis impairs recovery after spinal cord injury. J Exp Med. 2016;213:2603–20.
28. Hamad I, Van Broeckhoven J, Cardilli A, Hellings N, Strowig T, Lemmens S, Hendrix S, Kleinewietfeld M. Effects of recombinant IL-13 treatment on gut microbiota composition and functional recovery after Hemisection Spinal Cord Injury in mice. Nutrients. 2023;15:4148.
29. Lin R, Xu J, Ma Q, Chen M, Wang L, Wen S, Yang C, Ma C, Wang Y, Luo Q, Zhu N. Alterations in the fecal microbiota of patients with spinal cord injury. PLoS ONE. 2020;15:e0236470.
30. Rong Z, Huang Y, Cai H, Chen M, Wang H, Liu G, Zhang Z, Wu J. Gut Microbiota disorders promote inflammation and aggravate spinal cord Injury through the TLR4/MyD88 signaling pathway. Front Nutr. 2021;8:702659.
31. Haegeman B, Hamelin J, Moriarty J, Neal P, Dushoff J, Weitz JS. Robust estimation of microbial diversity in theory and in practice. Isme j. 2013;7:1092–101.
32. Kim BR, Shin J, Guevarra R, Lee JH, Kim DW, Seol KH, Lee JH, Kim HB, Isaacson R. Deciphering diversity indices for a better understanding of Microbial communities. J Microbiol Biotechnol. 2017;27:2089–93.
33. Bazzocchi G, Turroni S, Bulzamini MC, D'Amico F, Bava A, Castiglioni M, Cagnetta V, Losavio E, Cazzaniga M, Terenghi L, et al. Changes in gut microbiota in the acute phase after spinal cord injury correlate with severity of the lesion. Sci Rep. 2021;11:12743.
34. Ma Q, Xing C, Long W, Wang HY, Liu Q, Wang RF. Impact of microbiota on central nervous system and neurological diseases: the gut-brain axis. J Neuroinflammation. 2019;16:53.
35. Lee J, d'Aigle J, Atadja L, Quaicoe V, Honarpisheh P, Ganesh BP, Hassan A, Graf J, Petrosino J, Putluri N, et al. Gut microbiota-derived short-chain fatty acids promote poststroke recovery in aged mice. Circ Res. 2020;127:453–65.
36. Xiao W, Su J, Gao X, Yang H, Weng R, Ni W, Gu Y. The microbiota-gut-brain axis participates in chronic cerebral hypoperfusion by disrupting the metabolism of short-chain fatty acids. Microbiome. 2022;10:62.
37. Squair JW, Milano M, de Coucy A, Gautier M, Skinnider MA, James ND, Cho N, Lasne A, Kathe C, Hutson TH, et al. Recovery of walking after paralysis by regenerating characterized neurons to their natural target region. Science. 2023;381:1338–45.
38. Celorrio M, Abellanas MA, Rhodes J, Goodwin V, Moritz J, Vadivelu S, Wang L, Rodgers R, Xiao S, Anabayan I, et al. Gut microbial dysbiosis after traumatic

brain injury modulates the immune response and impairs neurogenesis. Acta Neuropathol Commun. 2021;9:40.
39. Liu C, Yang SY, Wang L, Zhou F. The gut microbiome: implications for neurogenesis and neurological diseases. Neural Regen Res. 2022;17:53–8.
40. Hellenbrand DJ, Quinn CM, Piper ZJ, Morehouse CN, Fixel JA, Hanna AS. Inflammation after spinal cord injury: a review of the critical timeline of signaling cues and cellular infiltration. J Neuroinflammation. 2021;18:284.
41. Popovich PG, Jones TB. Manipulating neuroinflammatory reactions in the injured spinal cord: back to basics. Trends Pharmacol Sci. 2003;24:13–7.
42. Erny D, Hrabě de Angelis AL, Jaitin D, Wieghofer P, Staszewski O, David E, Keren-Shaul H, Mahlakoiv T, Jakobshagen K, Buch T, et al. Host microbiota constantly control maturation and function of microglia in the CNS. Nat Neurosci. 2015;18:965–77.
43. Huang Y, Gao P, Qin T, Chu B, Xu T, Yi J, Wang Q, Yang Z, Jiang T, Fan J, et al. Delayed inhibition of collagen deposition by targeting bone morphogenetic protein 1 promotes recovery after spinal cord injury. Matrix Biol. 2023;118:69–91.
44. Sun X, Liu H, Tan Z, Hou Y, Pang M, Chen S, Xiao L, Yuan Q, Liu B, Rong L, He L. Remodeling microenvironment for endogenous repair through Precise Modulation of Chondroitin Sulfate proteoglycans following spinal cord Injury. Small. 2023;19:e2205012.
45. Kolb J, Tsata V, John N, Kim K, Möckel C, Rosso G, Kurbel V, Parmar A, Sharma G, Karandasheva K, et al. Small leucine-rich proteoglycans inhibit CNS regeneration by modifying the structural and mechanical properties of the lesion environment. Nat Commun. 2023;14:6814.
46. Qiu S, Deng PJ, He FL, Yan LW, Tu ZH, Liu XL, Quan DP, Bai Y, Zheng CB, Zhu QT. A decellularized nerve matrix scaffold inhibits neuroma formation in the stumps of transected peripheral nerve after peripheral nerve injury. Neural Regen Res. 2023;18:664–70.
47. Qiu W, Zhou B, Luo Y, Chen Y, Chen Z, Wu K, Wu H, Wu B, Guo J, Fang F. An optimized decellularized Extracellular Matrix from Dental Pulp Stem Cell sheets promotes axonal regeneration by multiple modes in spinal cord Injury rats. Adv Healthc Mater. 2025;14:e2402312.
48. Tan Z, Xiao L, Ma J, Shi K, Liu J, Feng F, Xie P, Dai Y, Yuan Q, Wu W, et al. Integrating hydrogels manipulate ECM deposition after spinal cord injury for specific neural reconnections via neuronal relays. Sci Adv. 2024;10:eado9120.
49. Fishbein SRS, Mahmud B, Dantas G. Antibiotic perturbations to the gut microbiome. Nat Rev Microbiol. 2023;21:772–88.
50. Liu C, Cheng X, Zhong S, Liu Z, Liu F, Lin X, Zhao Y, Guan M, Xiao T, Jolkkonen J, et al. Long-term modification of gut microbiota by broad-spectrum antibiotics improves stroke outcome in rats. Stroke Vasc Neurol. 2022;7:381–9.
51. Neo SH, Her Z, Othman R, Tee CA, Ong LC, Wang Y, Tan I, Tan J, Yang Y, Yang Z, et al. Expansion of human bone marrow-derived mesenchymal stromal cells with enhanced immunomodulatory properties. Stem Cell Res Ther. 2023;14:259.
52. Sun Z, Chen Z, Yin M, Wu X, Guo B, Cheng X, Quan R, Sun Y, Zhang Q, Fan Y, et al. Harnessing developmental dynamics of spinal cord extracellular matrix improves regenerative potential of spinal cord organoids. Cell Stem Cell. 2024;31:772–e787711.
53. Song S, Zhang G, Chen X, Zheng J, Liu X, Wang Y, Chen Z, Wang Y, Song Y, Zhou Q. HIF-1α increases the osteogenic capacity of ADSCs by coupling angiogenesis and osteogenesis via the HIF-1α/VEGF/AKT/mTOR signaling pathway. J Nanobiotechnol. 2023;21:257.
54. Zhao R, Wu X, Bi XY, Yang H, Zhang Q. Baicalin attenuates blood-spinal cord barrier disruption and apoptosis through PI3K/Akt signaling pathway after spinal cord injury. Neural Regen Res. 2022;17:1080–7.

Publisher's note